

Measuring the galaxy power spectrum with multiresolution
decomposition – II. diagonal and off-diagonal power spectra of the
LCRS galaxies

XiaoHu Yang^{1,2} Long-Long Feng^{1,2,3} YaoQuan Chu^{1,2} Li-Zhi Fang⁴

Received _____; accepted _____

arXiv:astro-ph/0102160v1 9 Feb 2001

¹Center for Astrophysics, University of Science and Technology of China, Hefei, Anhui
230026, P.R. China

²National Astronomical Observatories, Chinese Academy of Science, Chao-Yang District,
Beijing, 100012, P.R. China

³Institute for Theoretical Physics, Academy of Science, Beijing, 100080, P.R. China

⁴Department of Physics, University of Arizona, Tucson, AZ 85721

ABSTRACT

The power spectrum estimator based on the discrete wavelet transform (DWT) for 3-dimensional samples has been studied. The DWT estimator for higher than 1-dimensional samples provides two types of spectra with respect to diagonal and off-diagonal modes, respectively. The two types of modes have different spatial invariance, and therefore, the diagonal and off-diagonal DWT power spectra are very flexible to deal with configuration-related problems in the power spectrum detection. With simulation samples and the mock catalogues of the Las Campanas redshift survey (LCRS), we show 1. the slice-like geometry of the LCRS doesn't affect the off-diagonal power spectrum with "slice-like" mode; 2. the Poisson sampling with the LCRS selection function doesn't cause more than $1\text{-}\sigma$ error in the DWT power spectrum; and 3. the powers of the mass or galaxy random velocity fluctuations, which cause the redshift distortion, are approximately scale-independent. These results insure that the uncertainties of the power spectrum measurement are under control. The scatter of the DWT power spectra of the six strips of the LCRS survey is found to be rather small. It is less than $1\text{-}\sigma$ of the cosmic variance of mock sample in the wavenumber range $0.1 < k < 2 \text{ h Mpc}^{-1}$. To fit the detected LCRS diagonal DWT power spectrum with CDM models, we find that the best-fitting redshift distortion parameter β is about the same as that obtained from the Fourier power spectrum. The velocity dispersions σ_v for models SCDM and Λ CDM are also consistent with other σ_v detections with the LCRS. A systematic difference between the best-fitting parameters of diagonal and off-diagonal power spectra have been significantly measured. This indicates that the off-diagonal power spectra are capable of providing information about the power spectrum of the galaxy velocity field.

Subject headings: cosmology: theory - large-scale structure of universe

1. Introduction

The power spectrum is one of most important statistical measure to quantify the clustering features of large scale mass density distribution traced by galaxies. It directly reflects the physical scales of the processes that affect structure formation.

In paper I (Fang & Feng 2000), the method of measuring galaxy power spectrum with the multiresolution analysis of discrete wavelet transformation (DWT) is developed. It has been shown that the DWT analysis provides a lossless estimation of the power spectrum. The DWT power spectrum estimator is optimized in the sense that the spatial resolution automatically adapts to the perturbation wavelength under consideration. Since the DWT analysis has strong capability of suppressing the off-diagonal components of the covariance of density fluctuations, the DWT estimator is convenient to deal with data sets with a large volume and complex geometry. Moreover, the DWT estimator can fully avoid the alias effect which appears in usual binning schemes. Because Poisson process possesses diagonal covariance in the DWT representation, the Poisson sampling and selection effects on the power spectrum are suppressed to a minimum.

Besides these technical advantages of the computation of power spectrum, the DWT space-scale decomposition provides a physical insight into the clustering behavior in phase space, i.e. scale plus physical position. Even for second order statistics, i.e. the covariance of density fluctuations, the space-scale decomposition can reveal some clustering behaviors, such as two-point correlation in phase space, which can not be measured by decomposition with modes non-localized in phase space. Moreover, the covariance in DWT representation can avoid the difficulty caused by the central limit theorem (Fan & Bardeen 1995.)

The algorithm developed in Paper I is mainly for 1-D sample. Many algorithms for 1-D sample can directly be generalized into 3-D. A problem especially for 3-D DWT power spectrum estimator is on rotational invariance. 3-D DWT modes is given by the direct

product of 1-D DWT modes, and therefore, each of the 3-D DWT modes is described by three positive integers (j_1, j_2, j_3) corresponding to the scales of the mode in x_1 , x_2 and x_3 directions, respectively. Thus, there are two types of modes: diagonal mode with $j_1 = j_2 = j_3$; off-diagonal mode for which the three numbers (j_1, j_2, j_3) are not the same. The DWT estimator can provide two types of power spectra: 1. diagonal power spectrum given by the powers on diagonal modes, 2. off-diagonal power spectrum given by the powers on off-diagonal modes.

Because the two types of modes have different spatial invariance, the diagonal and off-diagonal DWT power spectra are very flexible to deal with configuration-related problems in the power spectrum detection. In this paper, we will study both diagonal and off-diagonal power spectra with the Las Campanas redshift survey galaxies, and relevant simulation samples and mock catalogues. The purpose is to demonstrate how the two types of power spectra are applied to estimate the uncertainties of power spectrum measurement caused by various anisotropies of the sample. It includes, for instance, the irregular geometry of the survey with very low filling factor, the scale-dependence of redshift distortion, and the inhomogeneity caused by the selection function. These results insure that the DWT estimator is capable of providing a stable measurement of the LCRS galaxy power spectrum and the best-fitting parameters of bias and velocity dispersion.

The paper is organized as follows. In §2, the DWT power spectrum estimator is briefly introduced with the emphasis on the property and algorithm for the off-diagonal DWT power spectrum. §3 describes the real and mock samples of galaxies. The applications of the diagonal and off-diagonal power spectra to the configuration-related problems are presented in §4. The results of the DWT power spectra of the LCRS, both diagonal and off-diagonal, and their error estimation are given in §5. The best-fitting values of the bias parameters and velocity dispersion are given in §5 as well. Finally, conclusions are stated in

§6.

2. DWT power spectrum estimator

2.1. The DWT decomposition of galaxy distributions

If the position measurement is perfectly precise, the observed galaxy number density distribution can be written as

$$n_g(\mathbf{x}) = \sum_{m=1}^{N_g} w_m \delta^D(\mathbf{x} - \mathbf{x}_m) \quad (1)$$

where coordinate $\mathbf{x} = (x_1, x_2, x_3)$, N_g is the total number of galaxies, \mathbf{x}_m is the position of the m th galaxy, w_m is its weight, and δ^D the 3-D Dirac δ function. Without loss of generality, we consider the sample which is contained in a spatial box with spatial ranges of $x_1 = 0 - L_1$, $x_2 = 0 - L_2$ and $x_3 = 0 - L_3$. It is not necessary that the box $L_1 L_2 L_3$ is fully filled by sample, i.e., allows $n_g(\mathbf{x}) = 0$ within some areas inside the box.

The observed galaxy number density distribution is considered to be a realization of a Poisson point process with an intensity $n(\mathbf{x}) = \bar{n}_g(\mathbf{x})[1 + \delta(\mathbf{x})]$, where $\bar{n}_g(\mathbf{x})$ is selection function, and $\delta(\mathbf{x})$ the density contrast fluctuation on the underlying matter field. The goal of power spectrum measurement is to estimate the power spectrum of the density fluctuations $\delta(\mathbf{x}) = [n(\mathbf{x})/\bar{n}(\mathbf{x})] - 1$ from the observed realization $\delta_g(\mathbf{x}) = [n_g(\mathbf{x})/\bar{n}_g(\mathbf{x})] - 1$.

Different power spectrum estimators adopt different decomposition of $\delta_g(\mathbf{x})$. The DWT decomposition is based on the orthogonal and complete set of 3-D wavelet basis $\{\psi_{\mathbf{j},1}(\mathbf{x})\}$, which can be constructed by a direct product of 1-D wavelet basis as

$$\psi_{\mathbf{j},1}(\mathbf{x}) = \psi_{j_1,l_1}(x_1)\psi_{j_2,l_2}(x_2)\psi_{j_3,l_3}(x_3), \quad (2)$$

where $j_i = 0, 1, 2..$ ($i = 1, 2, 3$) and $l_i = 0..2^{j_i-1}$. The wavelet $\psi_{\mathbf{j},1}(\mathbf{x})$ is localized in phase (scale and physical position) space, i.e. it is non-zero mainly in a volume

$L_1/2^{j_1} \times L_2/2^{j_2} \times L_3/2^{j_3}$, and around the position ($x_1 = l_1 L_1/2^{j_1}$, $x_2 = l_2 L_2/2^{j_2}$, $x_3 = l_3 L_3/2^{j_3}$) (Fang & Thews 1998.) The bases eq.(2) are orthonormal with respect both \mathbf{j} and \mathbf{l} , i.e.

$$\int \psi_{\mathbf{j},\mathbf{l}}(\mathbf{x}) \psi_{\mathbf{j}',\mathbf{l}'}(\mathbf{x}) d\mathbf{x} = \delta_{\mathbf{j},\mathbf{j}'}^K \delta_{\mathbf{l},\mathbf{l}'}^K,$$

where δ^K is the Kronecker Delta function.

The DWT decomposition of $[n_g(\mathbf{x})/\bar{n}_g(\mathbf{x})] - 1$ is then given by

$$\tilde{\epsilon}_{\mathbf{j}}^{\mathbf{l}} = \int \left[\frac{n_g(\mathbf{x})}{\bar{n}_g(\mathbf{x})} - 1 \right] \psi_{\mathbf{j},\mathbf{l}}(\mathbf{x}) d\mathbf{x}, \quad (3)$$

Since wavelets are admissible, i.e. $\int \psi_{\mathbf{j},\mathbf{l}}(x) dx = 0$, eq.(3) becomes

$$\tilde{\epsilon}_{\mathbf{j}}^{\mathbf{l}} = \int \frac{n_g(\mathbf{x})}{\bar{n}_g(\mathbf{x})} \psi_{\mathbf{j},\mathbf{l}}(\mathbf{x}) d\mathbf{x}. \quad (4)$$

Thus the fluctuations in galaxy number density can be described by the wavelet function coefficients (WFC) $\tilde{\epsilon}_{\mathbf{j}}^{\mathbf{l}}$, which is the density fluctuation on scale $\mathbf{j} = \{j_1, j_2, j_3\}$ localized at the position $\mathbf{l} = \{l_1, l_2, l_3\}$.

2.2. DWT power spectrum estimator

For a given scale \mathbf{j} , there are totally $2^{j_1+j_2+j_3}$ WFC variables. All second order statistics on the scale \mathbf{j} can be drawn from the covariance of these WFCs

$$C_{\mathbf{j}}^{\mathbf{l}\mathbf{l}'} = \tilde{\epsilon}_{\mathbf{j}}^{\mathbf{l}} \tilde{\epsilon}_{\mathbf{j}}^{\mathbf{l}'}. \quad (5)$$

It has been shown in Paper I that the power of the fluctuations on the modes with the scale index \mathbf{j} can be estimated by

$$P_{\mathbf{j}} = I_{\mathbf{j}}^2 - N_{\mathbf{j}}. \quad (6)$$

where

$$I_{\mathbf{j}}^2 = \frac{1}{2^{j_1+j_2+j_3}} \text{tr} C_{\mathbf{j}}^{\mathbf{l}\mathbf{l}'} = \frac{1}{2^{j_1+j_2+j_3}} \sum_{l_1=0}^{2^{j_1}-1} \sum_{l_2=0}^{2^{j_2}-1} \sum_{l_3=0}^{2^{j_3}-1} [\tilde{\epsilon}_{\mathbf{j}}^{\mathbf{l}}]^2, \quad (7)$$

and

$$N_{\mathbf{j}} = \frac{1}{2^{j_1+j_2+j_3}} \sum_{l_1=0}^{2^{j_1}-1} \sum_{l_2=0}^{2^{j_2}-1} \sum_{l_3=0}^{2^{j_3}-1} \int \frac{\psi_{\mathbf{j},1}^2(\mathbf{x})}{\bar{n}_g(\mathbf{x})} d\mathbf{x}. \quad (8)$$

The physical meaning of eq.(6) is clear. The term $I_{\mathbf{j}}^2$ is the mean power of \mathbf{j} modes measured from the observed realization $n_g(\mathbf{x})$, and the term $N_{\mathbf{j}}$ is the power on \mathbf{j} modes due to the Poisson noise. For a volume-limited survey, the mean galaxy density \bar{n}_g is independent of the redshift. The Poisson noise power is thus simply $1/\bar{n}_g$. $P_{\mathbf{j}}$ is usually referred to as the DWT power spectrum.

Paper I showed that for 1-D sample in space L the DWT power spectrum P_j is a band averaged Fourier spectrum given by

$$P_j = \frac{1}{2^j} \sum_{n=-\infty}^{\infty} |\hat{\psi}(n/2^j)|^2 P(n), \quad (9)$$

where $P(n)$ is the Fourier power spectrum with wavenumber $k = 2\pi n/L$ (for simplicity, we refer to n as the wavenumber below), and $\hat{\psi}(n)$ is the Fourier transform of the basic wavelet $\psi(\eta)$

$$\hat{\psi}(n) = \int_0^L \psi(\eta) e^{-i2\pi n\eta} d\eta. \quad (10)$$

which is orthogonal to the monopole, i.e. $\hat{\psi}(0) = 0$ and localized in wavenumber space. For the Daubechies 4 wavelet (Daubechies 1992), $|\hat{\psi}(n)|^2$ has symmetrically distributed peaks with respect to $n = 0$. The first highest peaks are non-zero in two narrow ranges centered at $n = \pm n_p$ with width Δn_p (see Fig. 1). Besides the first peak, there are “side lobes” in $|\hat{\psi}(n)|^2$ (see also Fig. 1). However, for the Daubechies 4 the area under the “side lobes” is not more than 2% of the first peak. Therefore P_j is good estimation of the band-averaged Fourier power spectrum centered at wavenumber

$$n_j = n_p 2^j, \quad (11)$$

with the band width as

$$\Delta n = 2^j \Delta n_p. \quad (12)$$

For 1-D sample of Ly α forests, the DWT power spectrum is found to be smoothly related to the Fourier power spectrum by eqs.(11) and (12) (Feng & Fang 2000.)

2.3. Diagonal and off-diagonal modes

It is straightforward to generalize eq.(9) to 3-D. We have

$$P_{\mathbf{j}} = \frac{1}{2^{j_1+j_2+j_3}} \sum_{n_1=-\infty}^{\infty} \sum_{n_2=-\infty}^{\infty} \sum_{n_3=-\infty}^{\infty} |\hat{\psi}(n_1/2^{j_1})\hat{\psi}(n_2/2^{j_2})\hat{\psi}(n_3/2^{j_3})|^2 P(n_1, n_2, n_3). \quad (13)$$

Because the cosmic density field is isotropic, the Fourier power spectrum $P(n_1, n_2, n_3)$ is dependent only on

$$n = \sqrt{n_1^2 + n_2^2 + n_3^2}. \quad (14)$$

Obviously, the DWT power spectrum is invariant with respect to the cyclic permutation of index as

$$P_{j_1, j_2, j_3} = P_{j_3, j_1, j_2} = P_{j_2, j_3, j_1} \quad (15)$$

Considering eq.(11) and (14), we can formally define a band center wavenumber n_j corresponding to the 3-D mode \mathbf{j} as

$$n_{\mathbf{j}} = n_p \sqrt{(2^{j_1})^2 + (2^{j_2})^2 + (2^{j_3})^2}. \quad (16)$$

For an isotropic random field, the Fourier modes with the same n [eq.(14)] are statistically equivalent. However, the DWT modes with the same n_j [eq.(16)] are not statistically equivalent, because the DWT modes are not rotationally invariant. A Fourier mode $e^{-i(2\pi/L)(n_1x_1+n_2x_2+n_3x_3)}$ can be obtained by a rotation of mode $e^{-i(2\pi/L)(n'_1x_1+n'_2x_2+n'_3x_3)}$ as long as $n_1'^2 + n_2'^2 + n_3'^2 = n_1^2 + n_2^2 + n_3^2$. However, the DWT modes don't have the same property. Generally, one cannot transform a mode (j_1, j_2, j_3) to (j'_1, j'_2, j'_3) by a rotation, even when $n_j \simeq n_{j'}$. Because of different configurations [eq.(2)] between them, the condition

$n_j = n_{j'}$ generally does not imply

$$P_{\mathbf{j}} = P_{\mathbf{j}'}. \quad (17)$$

This invariance holds only when (j_1, j_2, j_3) is a cyclic permutation of (j'_1, j'_2, j'_3) .

With this property, one can define two types of the DWT power spectra: 1. the diagonal power spectrum given by $P_{\mathbf{j}}$ on diagonal modes $j_1 = j_2 = j_3 = j$, and 2. off-diagonal power spectrum given by other modes.

From eq.(13), the diagonal power spectrum $P_j \equiv P_{j,j,j}$ is related to the Fourier power spectrum by

$$P_j = \sum_{n_1=-\infty}^{\infty} \sum_{n_2=-\infty}^{\infty} \sum_{n_3=-\infty}^{\infty} W_j(n_1, n_2, n_3) P(n_1, n_2, n_3), \quad (18)$$

where the window function W_j is

$$W_j(n_1, n_2, n_3) = \frac{1}{2^{3j}} |\hat{\psi}(n_1/2^j) \hat{\psi}(n_2/2^j) \hat{\psi}(n_3/2^j)|^2. \quad (19)$$

with the normalization

$$\int_{-\infty}^{\infty} W_j(n_1, n_2, n_3) dn_1 dn_2 dn_3 = 1 \quad (20)$$

It should be emphasized that the window function W_j does not contain any free parameters, and is completely determined by the basis used for the DWT decomposition. Therefore, it is different from the ordinary convolution with filter containing adjustable parameters.

Eq.(11) shows that in the scale space the window function W_j is localized around $n_1 = n_2 = n_3 = n_p 2^j$. Therefore, the diagonal power spectrum P_j is a band-average of the isotropic Fourier power spectrum $P(n)$ with the central frequency $n = \sqrt{3} n_g 2^j$. As an example, Fig. 1 demonstrates the linear diagonal DWT power spectra in three typical cosmological models, i.e. the Λ cold dark matter, (Λ CDM), τ CDM, and the standard CDM (SCDM). They are calculated by eq.(18), in which the $P(n)$ are taken to be the correspondingly linear isotropic Fourier power spectra (Bardeen et al. 1986). The wavelet filter $|\hat{\psi}(n)|^2$ [eq.(10)] is displayed in a small frame box.

For off-diagonal modes, one can also calculate the linear non-diagonal DWT power spectrum P_{j_1, j_2, j_3} via eq.(13.) However, in this case, P_{j_1, j_2, j_3} cannot simply be identified as a band average of the isotropic Fourier power spectrum $P(n)$ centered at $n = n_j$.

Nevertheless, n_j is useful to calibrate the physical scale of a given \mathbf{j} . Since we use the DWT decomposition, it is convenient to label the spatial scale in figures by j . However, the spatial scale for a given \mathbf{j} actually is dependent on the size of the sample L , i.e. $L/2^j$. Therefore, for samples with different L , the same j do not have the same physical scale. To avoid the possible confusion caused by this, we label the figures on the top with the wavenumber $k = 2\pi n_j/L$.

3. Samples

3.1. The LCRS galaxies

We use the Las Campanas redshift survey (Shectman et al. 1996) to demonstrate the DWT power spectrum estimator, including both diagonal and off-diagonal modes. The LCRS consists of 26418 redshifts of galaxies, covering over 720 square degree in six $1.5^\circ \times 80^\circ$ strips. Three each of the strips are in the north and south galactic caps, respectively. The galaxies in the LCRS are selected from a CCD catalog obtained in R-band. The luminosity function has been shown to be best-fitted by a Schechter function with $M^* = -20.29 \pm 0.02 + 5 \log h$, $\alpha = -0.70 \pm 0.05$ and $\phi^* = 0.019 \pm 0.001 \text{ h}^3 \text{Mpc}^{-3}$ for the absolute magnitude of $-23.0 \leq M - 5 \log h \leq -17.5$ (Lin et al. 1996.)

We first convert the heliocentric redshifts of galaxies to comoving distances r in a Einstein-de Sitter universe. As the survey depth is not very large, the differences among the distances given different models are less than 2%. This correction has been taken into account in our calculation. Analysis is carried out for the sample with upper cut-off of the

recession velocity 51000kms^{-1} , which is approximately the survey depth $\simeq 450 \text{ h}^{-1} \text{ Mpc}$. To perform DWT power spectrum analysis, we further enclose each strip into a cubic box with size of $500 \text{ h}^{-1} \text{ Mpc}$. Accordingly, the spatial size resolved by one-dimensional mode on a scale j is $500/2^j \text{ h}^{-1} \text{ Mpc}$.

A slice-like geometry of the strips fills only a very small fraction of the cubic volume. We define a filling factor by

$$f_s = \frac{V_s}{L_{box}^3} \quad (21)$$

where V_s is the volume occupied by the survey sample, and L_{box} is the length of the box. For a given scale $\mathbf{j} = (j_1, j_2, j_3)$, there are totally $N_{\mathbf{j}} = 2^{j_1+j_2+j_3}$ DWT modes. Since the wavelet $\psi_{j,l}$ is localized in physical space, the WFCs of modes located in the empty regions will be zero. Consequently, for the scale $\mathbf{j} = (j_1, j_2, j_3)$, only $f_s N_{\mathbf{j}}$ modes contribute to the DWT power spectrum. In this case, the summations overing l_1, l_2 and l_3 in eqs.(7) and (8) run only for the $f_s N_{\mathbf{j}}$ modes, and the normalization factor $1/2^{j_1+j_2+j_3}$ is replaced by $f_s N_{\mathbf{j}}$.

The effect of the boundary can be estimated with the so-called ‘‘influence’’ cone (Pando & Fang 1998.) That is, if the base $\psi_{j,l}(x)$ is well localized in the interval Δx , then the WFCs $\tilde{\epsilon}_{jl}$ corresponding to position x_0 will only measure fluctuations in the interval $[(x_0 - \Delta x)/2^j + 1, (x_0 + \Delta x)/2^{j+1}]$. If x_0 is at the boundary, the WFCs $\tilde{\epsilon}_{jl}$ measures the difference between the density contrasts inside and outside the boundary. Thus, for a zero padding of the empty regions, the power on the boundary mode would be statistically overestimated. Hence, the uncertainty (most likely overestimation) of the power spectrum caused by the boundary modes would be of the order of $N_{\mathbf{j}}^b/f_s N_{\mathbf{j}}$, where $N_{\mathbf{j}}^b$ is the number of boundary modes on scale \mathbf{j} . One can also pad the empty regions with galaxies created by a Poisson sampling according to the same radial selection function as the LCRS. In this case, the difference between the density contrasts inside and outside the boundary is erased, so contribute little to the DWT power spectrum and will cause small underestimation. For

small scales $N_j^b \ll f_s N_j$, the boundary effect is negligible for both zero padding and Poisson sampling.

3.2. N-body simulation and mock LCRS catalogues

To access the accuracy of recovering power spectrum with the DWT, we construct mock LCRS samples. First we produce ten realizations of the N-body simulation for each model of the standard cold dark matter model (SCDM), low density flat model (Λ CDM), and a variant of SCDM model (τ CDM). The parameters $(\Omega_0, \Lambda, \Gamma, \sigma_8)$ are taken to be $(1.0, 0.0, 0.5, 0.55)$ for SCDM, $(0.3, 0.7, 0.21, 0.85)$ for Λ CDM, and $(1.0, 0.0, 0.25, 0.55)$ for τ CDM. The linear power spectrum is taken from the fitting formula given in Bardeen et al. (1986). We use modified AP³M code (Couchman, 1991) to evolve 128^3 cold dark matter particles in a periodic cube of length $256h^{-1}\text{Mpc}$. For the SCDM model, the starting redshift is taken to be $z_i = 15$, and for LCDM and τ CDM, $z_i = 25$, respectively. The force softening parameter η in the comoving system decreases with time as $\eta \propto 1/a(t)$. Its initial value is taken to be $\eta = 384 h^{-1} \text{ kpc}$, and the minimum value to be $\eta_{\min} = 128 h^{-1} \text{ kpc}$, corresponding to 15% and 5%, respectively, of the grid size. For the single-step integration of time evolution, we use the “leap-frog” scheme, the total number of integration steps down to $z = 0$ is 600.

We first assume an unbiased galaxy distribution relative to underlying dark matter. The mock catalogues are then constructed proceeding in the following steps. 1. We locate the observer randomly in the simulation box. 2. Since the survey depth and width of the LCRS are larger than our simulations, we replicate the slice sample periodically be extending to redshift $z \sim 0.2$. 3. From the space coordinate of the galaxy, work out its redshift and galactic coordinates, for which the angular mask of the LCRS is further applied. 4. According to R-band luminosity function and the average sampling rates respectively

for 50-fiber and 112-fiber subset of the observation data, we determine whether the galaxy is admitted into the mock sample using Poisson sampling. Similar to the estimation of Fourier power spectrum in the LCRS catalogue (Lin et.al., 1996), the uneven sampling rate has little effect on measurements of the DWT Power spectrum. Finally in step 5, the photometric catalog is then generated by assigning each galaxy a specific absolute magnitude.

4. Estimating uncertainties with the DWT power spectrum

4.1. Diagonal power spectrum

In order to demonstrate the reliability of the DWT power spectrum estimator, we first calculate the diagonal DWT power spectrum for the simulation ensembles in the SCDM, Λ CDM, and τ CDM models. The sample is in a $256^3 \text{ h}^{-3} \text{ Mpc}^3$ box. The results are displayed in Fig. 2. For comparison, Fig. 2 also plots the non-linear DWT power spectrum calculated by Eq.(18), in which the Fourier power spectrum is taken from the Peacock & Dodds’s fitting formulae (1996.) Obviously, the DWT power spectrum estimator is excellent to recover the analytic models over a wide wavenumber range resolved by our simulations, i.e. $0.1 < k < 3 \text{ h Mpc}^{-1}$.

For the magnitude-limited mock samples of the LCRS in real space with size $500^3 \text{ h}^{-3} \text{ Mpc}^3$, the estimated diagonal DWT power spectrum are shown by solid squares in Fig. 3. The error bars are given by standard $1\text{-}\sigma$ deviations taken over 10 realizations. Comparing with the power spectrum calculated by Eq.(18), one finds that the DWT power spectrum estimator can successfully recover the non-linear spectra of the mass fields on scales $j > 3$, i.e., $k > 0.1 \text{ h Mpc}^{-1}$, while the power is systematically underestimated for $k < 0.1 \text{ h Mpc}^{-1}$

Recall that the Fourier power spectrum also shows a suppression of power spectrum on

large scales. It is generally believed that the suppression of the Fourier spectrum is due to the following two reasons: 1. the uncertainty in determination of mean density (Peacock & Nicholson 1991; Tadros & Efstathiou, 1996); 2. the finite volume of the survey.

The large scale suppression of the DWT power spectrum have different reasons. For the DWT power spectrum estimator, the overall mean density is not needed. The uncertainty of the mean density doesn't affect the DWT power spectrum. As a numerical test, we computed the DWT power spectrum in an arbitrary selected thin slab in the simulation box with the same filling factor as that of the LCRS. We found that the scatter of the DWT power spectra from different slabs is much less than the suppression shown in Fig. 2. Accordingly, the uncertainty of the overall mean density is *not* responsible for the suppression of the DWT power spectrum on large scales.

The suppression of the DWT power spectrum on large scales is because the diagonal mode (j, j, j) cannot match with the slice-like geometry of the survey. For the LCRS, the average thickness in declination is estimated to be $\sim 15 \text{ h}^{-1} \text{ Mpc}$, i.e. only $\sim 3\%$ of the side lengths in the other two dimensions. Therefore, the perturbations on scales $k < 0.2 \text{ h Mpc}^{-1}$, or $j \leq 3$, in the dimension of declination are poorly sampled. This leads to an underestimation of power spectrum with $j \leq 3$ in the direction of declination (§3.1). Based on above discussions, for mock samples with the LCRS survey geometry, the diagonal power spectrum $j_1 = j_2 = j_3 = j$ are capable of recovering the non-linear power spectrum on scales $j \geq 3$, but suffers an underestimation on scales $j \leq 3$. This geometric effect could also be fixed by the off-diagonal power spectrum as demonstrated in next subsection.

4.2. Slice-like geometry and off-diagonal power spectrum

Assuming that j_1 points along the direction of declination, j_2 the R.A. and j_3 the radial or redshift direction, the modes (j_1, j_2, j_3) which can fit with the LCRS' slice-like geometry are $2 \leq j_2, j_3 \leq 7$ and $4 \leq j_1 \leq 7$. We use the off-diagonal power spectrum P_{j_1, j_2, j_3} with a fixed $j_1 \geq 4$.

Figure 4 illustrates the off-diagonal DWT spectrum P_{5, j_2, j_3} measured from subsets of the sample in a $0.1L \times L \times L$ slab for SCDM and Λ CDM models respectively, in which redshift distortion and selection effect have not been taken into account. Clearly, it shows that the off-diagonal DWT power spectrum P_{5, j_2, j_3} estimator is capable of reproducing the non-linear power spectrum on large scales. This power spectrum is in good agreement with the theoretical curves on large scales as $k \simeq 0.5 \text{ h Mpc}^{-1}$.

Figure 5 plots the off-diagonal DWT spectra P_{4, j_2, j_3} and P_{5, j_2, j_3} in real space measured for the mock LCRS samples in the Λ CDM model. It again shows that the systematical underestimation of the powers on large scales is significantly erased. The off-diagonal DWT spectra P_{5, j_2, j_3} and P_{4, j_2, j_3} can be used for recovering the non-linear power spectrum of the mass field on scales as large as $k \simeq 0.15 \text{ h Mpc}^{-1}$.

4.3. Inhomogeneous effect of selection function

The purpose of introducing selection function $\bar{n}_g(r)$ is to eliminate the inhomogeneity and anisotropy of mean number density of galaxies caused by the sampling of the survey. That is, the distribution with uniformly mean number density of galaxies can be recovered by weighting a galaxy at radial coordinate $x_3 = r$ by factor $1/\bar{n}_g(r)$.

However, the effects of selection function actually are two-fold. On the one hand, it is to eliminate the inhomogeneity of the mean number density of the galaxy distribution. On

the other hand, it causes an inhomogeneity in the correlations of the power spectrum. The later can be seen from the band-band correlation in the Paper I, which showed that, if the selection function is slowly varying, the observed auto-correlation of power P_j is

$$\langle P_j P_j \rangle = \langle P_j P_j \rangle_I + \frac{1}{2^{2(j_1+j_2+j_3)}} \sum_{l_1=-0}^{2^{j_1}-1} \sum_{l_2=-0}^{2^{j_2}-1} \sum_{l_3=-0}^{2^{j_3}-1} \left[\frac{1}{\overline{\bar{n}_g^2(x_3)}} + \int \frac{\psi_{j,1}^4(\mathbf{x})}{\bar{n}_g^3(x_3)} d\mathbf{x} \right], \quad (22)$$

where $\langle P_j P_j \rangle_I$ is the power-power correlation before the Poisson sampling, and therefore, cyclic invariant with respect to (j_1, j_2, j_3) , i.e.

$$\langle P_{j_1, j_2, j_3} P_{j_1, j_2, j_3} \rangle_I = \langle P_{j_2, j_3, j_1} P_{j_2, j_3, j_1} \rangle_I = \langle P_{j_3, j_1, j_2} P_{j_3, j_1, j_2} \rangle_I. \quad (23)$$

The number $\overline{\bar{n}_g(x_3)}$ in eq.(22) is the mean of $\bar{n}_g(x_3)$ in cell (l_1, l_2, l_3) . Since $\bar{n}_g(x_3)$ depends only on x_3 , the last term in the r.h.s. of eq.(22) violates the permutation invariance. That is, the correlations $\langle P_{j_1, j_2, j_3} P_{j_1, j_2, j_3} \rangle$ are on longer cyclic invariant. In other words, the probability distribution function (PDF) of P_j is anisotropic.

To estimate this effect, we calculate the off-diagonal power spectra P_{4j4} and P_{44j} vs. j for Λ CDM simulation sample in real space, and the selection function is taken to be that for the LCRS galaxies, but in plane parallel approximation. The result is shown in Fig. 6. The two spectra P_{4j4} and P_{44j} show some difference, which is not significant on all scales $2 \leq j \leq 7$ within $1-\sigma$. Therefore, with the DWT estimator, the effect of the anisotropy given by the LCRS selection function can be ignored at least for the power measurement on scales similar to P_{4j4} and P_{44j} .

4.4. Redshift distortion and random velocity field of galaxies

Usually, the redshift distortion is considered to have two effects on the power spectrum measurement: 1. the enhancing of power on large scales due to the linear effect of redshift distortion; 2. the suppressing of power on small scales due to the random motions of

galaxies inside virialized groups and clusters of galaxies. The general theory of the two effects on the DWT power spectrum is given in Appendix. An interesting result is that the effect of the galaxy random velocity field $\mathbf{v}(\mathbf{x})$ upon the power on mode \mathbf{j} is mainly given by the power of the pairwise velocity dispersion of the same mode. Therefore, the DWT power spectrum can be employed for extracting information of the scale dependence of galaxy velocity fluctuations.

Recall that in the recovery of the real space Fourier power spectrum from redshift distorted measurement, it is usually assumed that the peculiar velocity dispersion is scale-independent. However, theory and measurement of galaxy pairwise velocity dispersion do not indicate a scale-independent, but weakly scale-dependent velocity field. Therefore, it is necessary to estimate the uncertainty caused by the assumption of the scale-independence of the velocity fluctuations.

Let's use the plane parallel approximation. In this case, the redshift distortion is determined by the x_3 -component of the galaxy velocity field, i.e. $v_3(\mathbf{x})$. Subjecting $v_3(\mathbf{x})$ to a DWT decomposition, we have

$$\tilde{\epsilon}_{\mathbf{j},\mathbf{l}}^V = \int v_3(\mathbf{x})\psi_{\mathbf{j},\mathbf{l}}(\mathbf{x})d\mathbf{x}. \quad (24)$$

The WFCs of the velocity field, $\tilde{\epsilon}_{\mathbf{j},\mathbf{l}}^V$, describes the radial velocity difference with spatial separation on scale \mathbf{j} at position \mathbf{l} . Therefore, it is the pairwise velocity on scale \mathbf{j} at position \mathbf{l} . The redshift distorted DWT power spectrum $P_{\mathbf{j}}^S$ is approximately given by (see Appendix §A.2)

$$P_{\mathbf{j}}^S \simeq \frac{1}{1 + S'_{\mathbf{j}}P_{\mathbf{j}}^V/H_0^2}P_{\mathbf{j}}, \quad (25)$$

where $S'_{\mathbf{j}}$ is determined by the geometry of the mode \mathbf{j}

$$S'_{\mathbf{j}} = \int \psi_{\mathbf{j},\mathbf{l}}^2 \left(\frac{\partial \psi_{\mathbf{j},\mathbf{l}}}{\partial x_3} \right)^2 d\mathbf{x}, \quad (26)$$

and $P_{\mathbf{j}}^V$ is the power of the pairwise velocity dispersion on scale \mathbf{j} , i.e.

$$P_{\mathbf{j}}^V = \langle |\tilde{\epsilon}_{\mathbf{j},1}^V|^2 \rangle_v. \quad (27)$$

Therefore, comparing $P_{\mathbf{j}}^S$ with $P_{\mathbf{j}}$, we are able to determine $P_{\mathbf{j}}^V$.

As an example, we study the assumption of the scale-independence of galaxy velocity fluctuations. One can show that, if the power of pairwise velocity is scale-independent, we have

$$S'_{j_1, j_2, j_3} P_{j_1, j_2, j_3}^V \simeq \text{const}, \quad \text{for a fixed } j_3 \quad (28)$$

Therefore, the scale-dependence of the velocity fluctuations can be detected by off-diagonal DWT power spectrum with a fixed j_3 (redshift direction). Figure 7 plots $P_{4,j,4}$ vs. j in redshift space for the Λ CDM simulation samples. It can be seen clearly from Fig. 7 that the DWT power spectrum $P_{4,j,4}$ in redshift space is almost parallel to the theoretical non-linear spectrum in real space. The difference between the redshift distortion suppressions of mode $(4, 2, 4)$ and $(4, 7, 4)$ is no more than a factor of 2. That is, the suppressing factor $1/(1 + S'_{\mathbf{j}}) \simeq \text{const}$, and therefore eq.(28) approximately hold in the scale range of spectrum $P_{4,j,4}$. Similar results are obtained for models SCDM and τ CDM models. The assumption of a scale independent power of the pairwise velocity seems to be reasonable at least for the DWT power spectrum of the LCRS sample.

Figure 7 also presents the off-diagonal power spectra $P_{4,4,j}$. Obviously, $P_{4,4,j}$ significantly differs from $P_{4,j,4}$ in both shape and amplitude of the power. Comparing to $P_{4,j,4}$, the amplitude of $P_{4,4,j}$ is enhanced on large scales and suppressed on small scales.

The difference between the spectra $P_{4,j,4}$ and $P_{4,4,j}$ in redshift space is worth while to look at. For an isotropic velocity field, P_{j_1, j_2, j_3}^V is cyclically invariant with respect to the index (j_1, j_2, j_3) , i.e.,

$$P_{4,4,j}^V = P_{4,j,4}^V. \quad (29)$$

The difference between $P_{4,4,j}$ and $P_{4,j,4}$ is simply given by the geometric factors S'_j , which are not cyclically invariant

$$\begin{aligned} S'_{4,4,j} &> S'_{4,j,4} & j > 4; \\ S'_{4,4,j} &< S'_{4,j,4} & j < 4 \end{aligned} \tag{30}$$

Therefore, using the difference between $P_{4,4,j}$ and $P_{4,j,4}$ in redshift space we are able to directly measure the power spectrum of galaxy velocity field, $P_{4,4,j}^V$ or $P_{4,j,4}^V$.

5. The DWT power spectrum of LCRS galaxies

5.1. The diagonal DWT power spectrum

With the preparations given in last sections, we can measure the DWT power spectrum of the LCRS galaxies. As discussed in §4.1, the diagonal power spectrum could provide a robust measurement of the non-linear power spectrum on scales of $k > 0.1 \text{ h Mpc}^{-1}$. In Fig. 8, we present the results for the LCRS, where the diagonal DWT power spectra measured in the six slices are plotted by scatter symbols as indicated in the figure. The average value over the six strips, and over the three north as well as three south strips are also displayed by the connected lines, respectively.

Although the geometry of the six strips are actually quite different, and the filling factor is only about 0.9%, Fig. 8 indicates that the scatter of the power on scales of $0.1 < k < 2 \text{ h Mpc}^{-1}$ is rather small. Comparing with Fig. 3, we find that the scatter of the power in Fig. 8 is within the range of $1\text{-}\sigma$ deviations given by the mock LCRS samples. Therefore, most of the scatters in Fig. 8 are probably from the cosmic variance. This result implies that the DWT power spectrum estimator is insensitive to the geometry of survey and filling factor. This feature allows us to directly compare the DWT power spectrum measurements from different surveys, or different region in a survey.

As indicated in Fig. 8, the DWT power spectrum is capable of probing the fluctuation power on scales as small as $k = 2 \text{ h Mpc}^{-1}$ ($j = 7$). This is partially because the DWT decomposition is free from the “aliasing effect” which may lead to underestimation of power on the scale of grid size (Jing 1992, Baugh & Efstathiou, 1994). At the scale $j = 6$, the number of effective modes is $f_s N_j \simeq 2500$ comparable to galaxy number in each slice, and thus the error bars for $j \geq 6$ are mainly from the Poisson noise. Even on the smallest scale $j = 7$ the Poisson correction is still much smaller than the detected power. Therefore, the diagonal DWT power spectrum from $k \simeq 0.1$ to 2 h Mpc^{-1} is qualified for model discrimination.

5.2. Fitting values of the bias parameter and velocity dispersion

In order to find the best values of the bias parameter and velocity dispersion, we compare the detected LCRS diagonal DWT power spectrum (Fig. 8) with the fitting spectrum in redshift space, P_j^S , given by eq.(13), i.e.

$$P_j^S = \frac{1}{2^{j_1+j_2+j_3}} \sum_{n_1=-\infty}^{\infty} \sum_{n_2=-\infty}^{\infty} \sum_{n_3=-\infty}^{\infty} |\hat{\psi}(n_1/2^{j_1})\hat{\psi}(n_2/2^{j_2})\hat{\psi}(n_3/2^{j_3})|^2 P^S(n_1, n_2, n_3), \quad (31)$$

where $P^S(n_1, n_2, n_3)$ is the Fourier power spectrum in redshift space. For typical CDM models, $P^S(n_1, n_2, n_3)$ can be taken from the fitting formula given by Peacock and Dodds (1994). It is

$$P^S(k) = b^2 P_m(k) G(\beta, k\sigma_v) \quad (32)$$

where $P_m(k)$ is the non-linear mass power spectrum in real space, $\beta = \Omega^{0.6}/b$ is redshift distortion parameter, b the scale-independent linear biasing parameter, σ_v is 1-D peculiar velocity dispersion. $G(\beta, k\sigma_v)$ describes the suppression of redshift distortion.

Exactly speaking, one cannot simply generalize eq.(13) to eq.(31), because the redshift distortion of the DWT power spectrum is different from the Fourier power spectrum. The

pairwise velocity suppression of the DWT modes should be calculated based on eq.(25), rather than via the Fourier modes. Moreover, eq.(32) is given by averaging over the directions of Fourier modes, and therefore, it doesn't match the anisotropic mode (j_1, j_2, j_3) of eq.(31). Nevertheless, the fitting of eq.(31) will provide worth information for diagonal modes, as the power of the galaxy random velocity field is approximately scale-independent (§4.4).

We treat b and σ_v in eq.(31) as free parameters, and fit the power spectrum eq.(31) to the detected DWT power spectrum of LCRS. The result is shown in Fig. 9, in which the $1\text{-}\sigma$ error bars of the observed DWT power spectrum are given by the scatter over the observed 6 slices themselves. As have been discussed in §4.1, the DWT power spectrum at large scales ($j \leq 3$) are underestimated due to the slice-like geometric effect. We approximately compensate this effect in the observed DWT power spectrum by using the fractional damping of amplitude calculated from the mock samples in redshift space relative to the expected values from the non-linear fitting formula (Eq.(32)) in each model respectively. The least square best fitting parameters b and σ_v for each of models are presented in Table 1.

The SCDM and Λ CDM parameter β given in the Table 1 is about the same as other measurements, such as $\beta = 0.52 \pm 0.13$ for the 1.2Jy IRAS survey (Cole et al. 1995);

Table 1

Model	b	$\beta(P_{jjj})$	$\beta(P_{5jj})$	$\sigma_v \text{ km s}^{-1} (P_{jjj})$	$\sigma_v \text{ km s}^{-1} (P_{5jj})$
SCDM	1.78 ± 0.30	0.56 ± 0.09	0.50	306 ± 106	397
τ CDM	1.50 ± 0.18	0.67 ± 0.08	0.59	135 ± 42	217
Λ CDM	1.06 ± 0.13	0.46 ± 0.06	0.41	250 ± 72	344

$\beta = 0.47 \pm 0.16$ (Tadros et al. 1999) and $\beta = 0.41_{-0.12}^{+0.13}$ (Hamilton et al. 2000) for IRAS Point Source Catalog Redshift Survey (PSCz). Actually, our estimated β in each CDM model is very close to the linear value $\sigma_8 \Omega_0^{0.6}$. This result is consistent with the theory of redshift distortion in the DWT presentation, which shows that the linear effect on the diagonal DWT power spectrum is about the same as that given by eq.(32) (see, Appendix §A.1.)

The 1-D velocity dispersions given in Table 1 look lower than other measurements in the LCRS galaxies. They are $v_{12} = 570 \pm 80 \text{ km s}^{-1}$ (Jing et al. 1998), and $363 \pm 13 \text{ km s}^{-1}$ (Landy, Szalay and Broadhurst 1998). Yet, the first measurement is based on *a priori* infall model of galaxies. In the second measurement v_{12} is given by the width of an exponential distribution, or a Lorentzian distribution in k space. On the other hand, σ_v in eq.(31) is assumed to be the variance of a Gaussian distribution of pairwise velocity. To fit a given power suppression by Lorentzian and Gaussian distributions, v_{12} will always be larger than σ_v . For instance, if the suppression factor is equal to about 3 as shown by the spectra of Fig. 7. v_{12}/σ_v will be ~ 1.4 . Therefore, the values of σ_v given by the fitting of the SCDM and Λ CDM basically are consistent with the second measurement.

5.3. Off-diagonal DWT power spectrum

As an example we detected the off-diagonal spectrum P_{5jj} of the LCRS galaxies. The result is presented in Fig. 10.

As mentioned in last section, eq.(31) cannot be used to fit with off-diagonal DWT power spectrum, as $P^S(k)$ is isotropic. One can expect that the fitting parameters of the spectrum eqs.(31) and (32) with an off-diagonal power spectrum would be systematically different from those of the diagonal power spectrum. This systematic difference actually

contains valuable information. The best fitted spectra of P_{5jj} for models SCDM, τ CDM and Λ CDM are also shown in Fig. 10. The best-fitting parameters are given in Table 1, which clearly show the difference between the parameters of diagonal and off-diagonal spectrum. Now we analyze the physical meaning of the difference.

From Appendix A.1, the linear redshift distortion of spectrum P_j is determined by the factor βS_j , where S_j is a geometric factor given by eq.(A4). The linear redshift distortion is significant on large scale. Moreover, the geometric factor satisfies

$$S_{5jj} < S_{jjj} \quad \text{for } j < 5. \quad (33)$$

Therefore the spectrum P_{5jj} is less affected by the linear redshift distortion than P_{jjj} . Thus, if fitting both P_{jjj} and P_{5jj} with the *same* fitting formula eq.(31), the best-fitting β for P_{5jj} will be lower than those of P_{jjj} . Table 1 shows the systematic lowering of $\beta(P_{5jj})$ than $\beta(P_{jjj})$.

The effect of galaxy pairwise velocity on spectrum P_j is determined by the power $P_j^V S_j'$ (Appendix A.2). If the power of pairwise velocity is approximately scale-independent, we have

$$P_{5jj}^V S_{5jj}' > P_{jjj}^V S_{jjj}'. \quad (34)$$

That is, the spectrum P_{5jj} is strongly affected by the random velocity field than P_{jjj} . Thus, if fitting both P_{jjj} and P_{5jj} with the same fitting formula eq.(31), the best-fitting σ_v for P_{5jj} will be larger than those of P_{jjj} . This is shown in Table 1. The significant difference between the best-fitting results of P_{jjj} and P_{5jj} shows that the off-diagonal power spectrum has the capability of measuring the galaxy velocity field from the observational data.

6. Conclusions

The DWT power spectrum estimator is studied with the galaxy distributions of the Las Campanas redshift survey, and the relevant mock and simulation samples in models of the SCDM, τ CDM and Λ CDM.

The DWT estimator for 3-D samples provide two types of spectra with respect to diagonal and off-diagonal modes, respectively. The two types of the DWT local modes have different configuration and invariance, and therefore, the diagonal and off-diagonal DWT power spectra are flexible for studying direction-dependent properties.

Using mock and simulation samples, we studied the effect of the irregular geometry of the survey, the inhomogeneity caused by the selection function, the scale-dependence of the redshift distortion due to the random velocity field of galaxies etc. To estimate the uncertainty and errors caused by these effects, the localization of the DWT modes in phase space are essential. For instance, the off-diagonal power spectra are capable of measuring the statistical features of the random velocity field of galaxies on mode \mathbf{j} , because the DWT power on mode \mathbf{j} is mainly affected by the power of the velocity fluctuations on mode \mathbf{j} .

The DWT power spectrum from the six slices of the LCRS galaxies are very stable over the scale range $0.06 \leq k \leq 2.0h \text{ Mpc}^{-1}$, in spite of the fact that the filling factor of the LCRS galaxies is only about 0.9% (in comparison, SDSS’s filling factor is about 17%.) To fit the LCRS DWT power spectrum with CDM models, we find that the redshift distortion parameter β and the 1-D velocity dispersion σ_v are consistent with results of the Fourier power spectrum. Therefore, the DWT estimator can give a robust measurement of the banded Fourier power spectrum.

More interesting, the differences between the best-fitting parameters of LCRS’ diagonal and off-diagonal DWT power spectra are found to be significant. This shows that the

redshift space behaviors of the diagonal and off-diagonal DWT power spectra are different. With the diagonal and off-diagonal DWT power spectra, we would be able to compare the pairwise velocity dispersion on different modes. Therefore, the difference between diagonal and off-diagonal power spectra would be valuable to constrain models.

LLF and YQC acknowledges support from the National Science Foundation of China (NSFC) and National Key Basic Research Science Foundation. We thank anonymous referee for helpful comments.

A. Redshift distortion in the DWT representation

A.1. Linear redshift distortion

If the density field is viewed in redshift space, the observed radial position is given by the radial velocity consisting of the uniform Hubble flow and the peculiar motion $\mathbf{v}(\mathbf{x})$. In the linear regime of clustering, the effect of redshift distortion can be described by a linear mapping from density contrast $\delta(\mathbf{x})$ in real space to redshift space

$$\delta^S(\mathbf{x}) = \mathbf{S}\delta(\mathbf{x}), \tag{A1}$$

where \mathbf{S} is the linear redshift distortion operator. In plane-parallel approximation, it is

$$\mathbf{S} = 1 + \beta \frac{\partial^2}{\partial x_3^2} \nabla^{-2}, \tag{A2}$$

where β is the redshift distortion parameter, and x_3 is on the direction of redshift.

The differential operator in eq.(A2) is quasi-diagonal when decomposed into the DWT basis (Farge et al. 1996.) Thus, similar to eqs.(2) and (3), $\delta^S(\mathbf{x})$ can be decomposed into

$$\tilde{\epsilon}_{\mathbf{j}}^{S,1} \simeq (1 + \beta S_{\mathbf{j}}) \tilde{\epsilon}_{\mathbf{j}}^1, \tag{A3}$$

where the coefficient $S_{\mathbf{j}}$ is given by

$$S_{\mathbf{j}} = \int \psi_{\mathbf{j},\mathbf{l}}(\mathbf{x}) \frac{\partial^2}{\partial x_3^2} \nabla^{-2} \psi_{\mathbf{j},\mathbf{l}}(\mathbf{x}) d\mathbf{x}. \quad (\text{A4})$$

This integral is independent of \mathbf{l} . For diagonal modes $\mathbf{j} = (j, j, j)$, we have

$$S_{jjj} = 1/3. \quad (\text{A5})$$

Using eqs.(5) and (6), the relation between the DWT power spectra in redshift space, $P_{\mathbf{j}}^S$ and real space $P_{\mathbf{j}}$ is given by

$$P_{\mathbf{j}}^S = (1 + \beta S_{\mathbf{j}})^2 P_{\mathbf{j}}. \quad (\text{A6})$$

For diagonal DWT power spectrum, we have

$$P_{jjj}^S = (1 + \frac{1}{3}\beta)^2 P_{jjj}. \quad (\text{A7})$$

The redshift distortion of the Poisson correction are not considered in eqs.(6) and (7).

The precise theory of the redshift distortion of the Poisson correction requires to calculate the selection function by the DWT decomposition. We will not give it here. In a rough approximation, the effect of the Poisson correction can be estimated by

$$P_{\mathbf{j}}^S = (1 + \beta S_{\mathbf{j}})^2 I_{\mathbf{j}}^2 - N_{\mathbf{j}} = (1 + \beta S_{\mathbf{j}})^2 (P_{\mathbf{j}} + N_{\mathbf{j}}) - N_{\mathbf{j}}. \quad (\text{A8})$$

A.2. Effect of random velocity field

In non-linear regime of clustering, the redshift distortion generally is estimated by assuming a random velocity field $\mathbf{v}(\mathbf{x})$, which describe the velocity dispersion of galaxies. The average of $\mathbf{v}(\mathbf{x})$ is zero, $\langle \mathbf{v}(\mathbf{x}) \rangle_v = 0$, where $\langle \dots \rangle_v$ is for the average over ensemble of velocity fields. The covariance of the density contrast in redshift space is then given by

$$\langle \langle \delta(x_1, x_2, x_3 + v_3(\mathbf{x})/H_0) \delta(x'_1, x'_2, x'_3 + v_3(\mathbf{x}')/H_0) \rangle_v \rangle, \quad (\text{A9})$$

Thus, the DWT power spectrum in redshift space is

$$P_{\mathbf{j}}^S = \langle \langle [\tilde{\epsilon}_{\mathbf{j}}^{S,1}]^2 \rangle \rangle_v - N_{\mathbf{j}}, \quad (\text{A10})$$

where

$$\tilde{\epsilon}_{\mathbf{j}}^{S,1} = \int \delta(x_1, x_2, x_3 + v_3(\mathbf{x})/H_0) \psi_{\mathbf{j},1}(\mathbf{x}) d\mathbf{x}. \quad (\text{A11})$$

Using an auxiliary variable J , eq.(A10) can be rewritten as

$$\tilde{\epsilon}_{\mathbf{j}}^{S,1} = \int d\mathbf{x} \delta\left(x_1, x_2, x_3 - i\frac{\delta}{\delta J}\right) e^{iJv_3(\mathbf{x})/H_0} \psi_{\mathbf{j},1}(\mathbf{x}) \Big|_{J=0}. \quad (\text{A12})$$

Thus, we have

$$\begin{aligned} \langle \langle [\tilde{\epsilon}_{\mathbf{j}}^{S,1}]^2 \rangle \rangle_v = & \quad (\text{A13}) \\ & \int d\mathbf{x} d\mathbf{x}' \delta\left(x_1, x_2, x_3 - i\frac{\delta}{\delta J}\right) \delta\left(x'_1, x'_2, x'_3 - i\frac{\delta}{\delta J'}\right) \\ & \langle e^{iJv_3(\mathbf{x})/H_0 + iJ'v_3(\mathbf{x}')/H_0} \rangle_v \psi_{\mathbf{j},1}(\mathbf{x}) \psi_{\mathbf{j},1}(\mathbf{x}') \Big|_{J, J'=0} \end{aligned}$$

In the lowest order of non-zero correction, we have

$$\begin{aligned} \langle e^{iJv_3(\mathbf{x})/H_0 + iJ'v_3(\mathbf{x}')/H_0} \rangle_v \simeq & \quad (\text{A14}) \\ 1 - \frac{1}{2H_0^2} [J^2 \langle v_3^2(\mathbf{x}) \rangle_v + J'^2 \langle v_3^2(\mathbf{x}') \rangle_v + 2JJ' \langle v_3(\mathbf{x}) v_3(\mathbf{x}') \rangle_v] \end{aligned}$$

In this case, the redshift distorted power spectrum is

$$P_{\mathbf{j}}^S = \left(1 - \frac{1}{H_0^2} S'_{\mathbf{j}} \langle |\tilde{\epsilon}_{\mathbf{j},1}^V|^2 \rangle_v\right) P_{\mathbf{j}}, \quad (\text{A15})$$

where $\tilde{\epsilon}_{\mathbf{j},1}^V$ is the WFCs of velocity field, i.e.

$$\tilde{\epsilon}_{\mathbf{j},1}^V = \int v_3(\mathbf{x}) \psi_{\mathbf{j},1}(\mathbf{x}) d\mathbf{x}. \quad (\text{A16})$$

The geometry factor $S'_{\mathbf{j}}$ is positive, and is given by

$$S'_{\mathbf{j}} = \int \psi_{\mathbf{j},1}^2 \left(\frac{\partial \psi_{\mathbf{j},1}}{\partial x_3} \right)^2 d\mathbf{x} \quad (\text{A17})$$

When the correction term is large, we have an approximation as

$$P_{\mathbf{j}}^S \simeq \frac{1}{1 + S'_{\mathbf{j}} \langle |\tilde{\epsilon}_{\mathbf{j},\mathbf{l}}^V|^2 \rangle_v / H_0^2} P_{\mathbf{j}}, \quad (\text{A18})$$

If the velocity field is homogeneous and isotropic, $\langle |\tilde{\epsilon}_{\mathbf{j},\mathbf{l}}^V|^2 \rangle_v$ is \mathbf{l} -independent. It is the power of velocity fluctuations on scale \mathbf{j} , i.e.

$$P_{\mathbf{j}}^V = \langle |\tilde{\epsilon}_{\mathbf{j},\mathbf{l}}^V|^2 \rangle_v. \quad (\text{A19})$$

Thus, we have

$$P_{\mathbf{j}}^S \simeq \frac{1}{1 + S'_{\mathbf{j}} P_{\mathbf{j}}^V / H_0^2} P_{\mathbf{j}}. \quad (\text{A20})$$

Therefore, the effect of the galaxy random velocity field upon the power $P_{\mathbf{j}}$ on scales \mathbf{j} is mainly given by the power of the v_3 fluctuations on the same scale.

Similar to eq.(A8), the redshift distortion of the Poisson correction can be estimated by

$$P_{\mathbf{j}}^S = \left(1 - \frac{1}{H_0^2} S'_{\mathbf{j}} \langle |\tilde{\epsilon}_{\mathbf{j},\mathbf{l}}^V|^2 \rangle_v \right) (P_{\mathbf{j}} + N_{\mathbf{j}}) - N_{\mathbf{j}}. \quad (\text{A21})$$

REFERENCES

- Bardeen, J.M., Bond, J.R., Kaiser, N. & Szalay, A.S., 1986, ApJ, 304, 15
- Baugh, C.M., & Efstathiou, G., 1994, MNRAS, 270, 183
- Cole, S., Fisher, K.B. & Weinberg, D.H., 1995, MNRAS, 275, 515
- Couchman, H.M.P., 1991, ApJ, 368, 23
- Daubechies I. 1992, Ten Lectures on Wavelets, (Philadelphia, SIAM)
- Fan, Z.H. & Bardeen, J. M. 1995 Phys. Rev. D, 51, 6714
- Fang, L.Z. & Thews, R. 1998, Wavelet in Physics, (World Scientific, Singapore)
- Fang, L.Z. & Feng, L.L. 2000, ApJ, 539,5
- Farge, M. Kevlahan, N., Perrier, V. & Goirand, E. 1996, Proceedings of the IEEE, 84, 639
- Feng, L.L. & Fang, L.Z. 2000, ApJ, 535,519
- Hamilton, A.J.S., Tegmark, M. & Padmanabhan, N.,2000 astro-ph/0004334
- Jing, Y.P., 1992, PhD thesis
- Jing Y.P., Mo, H.J., & Borner G., 1998, ApJ, 494 1
- Landy, S.D., Szalay, A.S., & Broadhurst, T.J. 1998, ApJ, 494, L133.
- Lin, H., Kirshner, P., Shectman, S.A., Landy, S.D., Oemler, A., Tucker, D.L. & Schechter, P.L., 1996, ApJ, 464, 60L
- Pando, J. & Fang, L.Z. 1998, Phys. Rev. E57, 3593
- Peacock, J.A. & Dodds, S.J., 1994, MNRAS, 167, 1020

Peacock, J.A. & Dodds, S.J., 1996, MNRAS, 280, L19

Peacock, J.A., & Nicholson, D., 1991, MNRAS, 253, 307

Shethman, S.A., Landy, S.D., Oemler, A., Tucker, D.L., Lin, H., Kirshner, R.P. & Schechter, P.L., 1996, ApJ 470, 172,

Tados H. & Efstathiou G. 1996, MNRAS 282 1381

Tadros H., Ballinger W. E., Taylor A. N., Heavens A. F., Efstathiou G., Saunders W., Frenk C. S., Keeble O., McMahon R., Maddox S. J., Oliver S., Rowan-Robinson M., Sutherland W. J., White S. D. M., 1999, MNRAS 305, 527

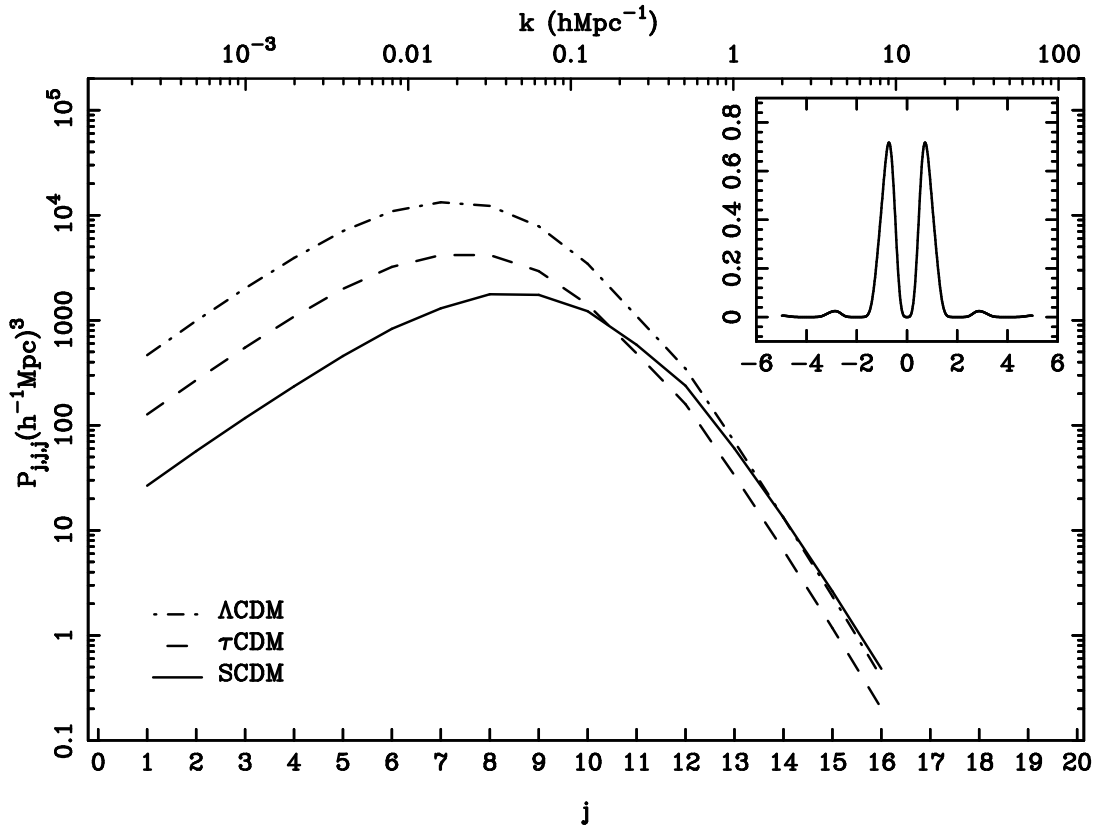


Fig. 1.— Linear diagonal DWT power spectrum in three typical cosmological models: ΛCDM , τCDM and SCDM . The wavelet filter $|\hat{\psi}(n)|^2$ is displayed in a small frame.

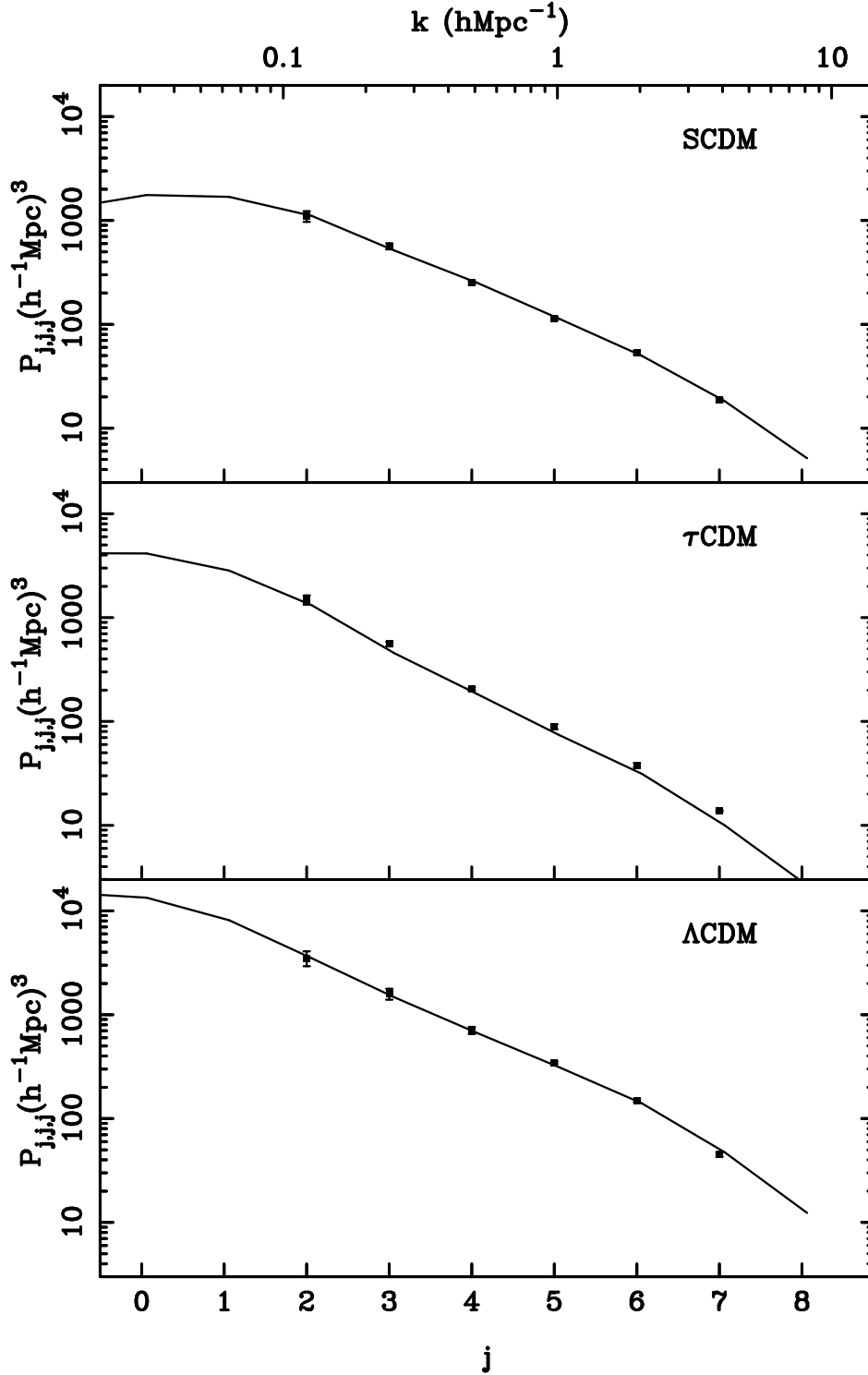


Fig. 2.— The non-linear diagonal DWT power spectrum of simulation samples (solid square) and the corresponding DWT power spectrum (solid line) calculated by eq.(18), in which the non-linear Fourier power spectrum $P(n_1, n_2, n_3)$ are taken from Peacock & Dodds’s fitting formulae (1994). The error bars are given by 1- σ deviations obtained from 10 realizations.

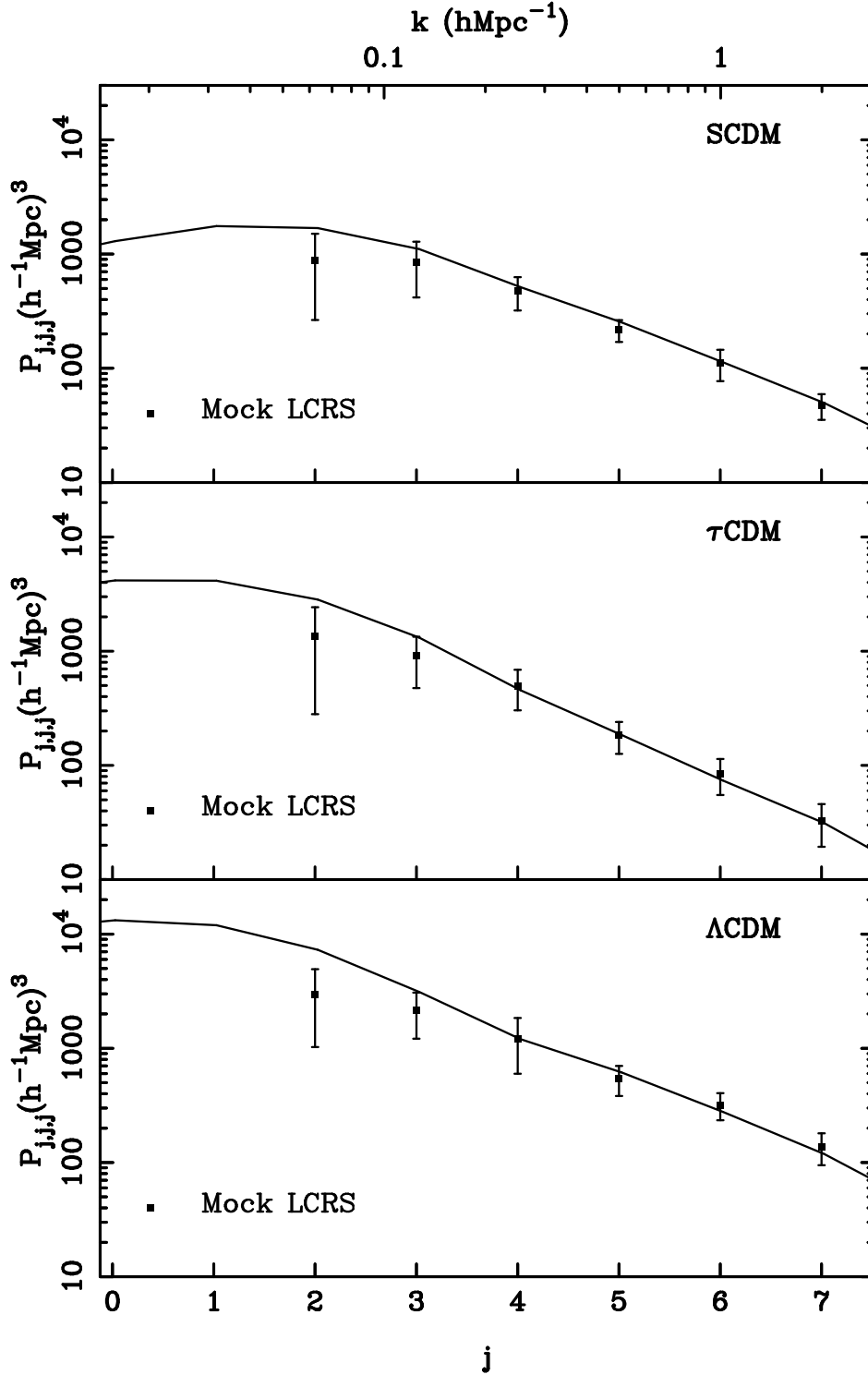


Fig. 3.— The diagonal DWT power spectrum of the mock flux limited LCRS catalogue in real space for models SCDM (upper panel), τ CDM (central panel) and Λ CDM (lower panel). The non-linear DWT power spectra (solid line) are calculated by eq.(18), in which the Fourier spectrum $P(n_1, n_2, n_3)$ is taken from the Peacock-Dodds fitting formulae. The non-linear DWT power spectra are calculated from 16 realizations of mock catalogues.

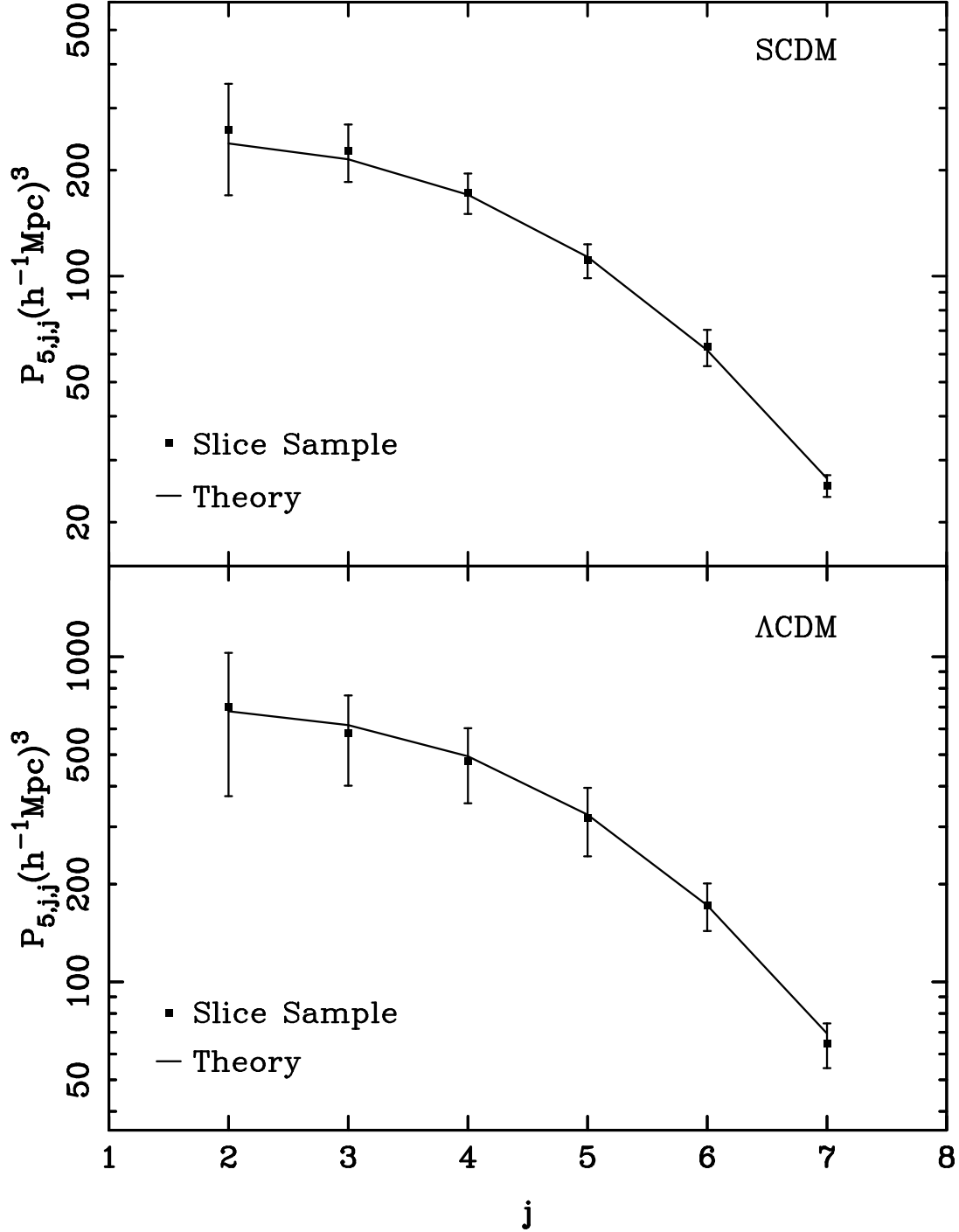


Fig. 4.— The off-diagonal DWT spectrum $P_{5,j,j}$ for SCDM and Λ CDM simulation slice samples in real space. Selection effect is not applied. The dimension in x -axis is thin ($x = 0.1L$). The solid line is the spectrum calculated by eq.(13), in which the Fourier spectrum $P(n_1, n_2, n_3)$ is taken from the Peacock-Dodds fitting formulae.

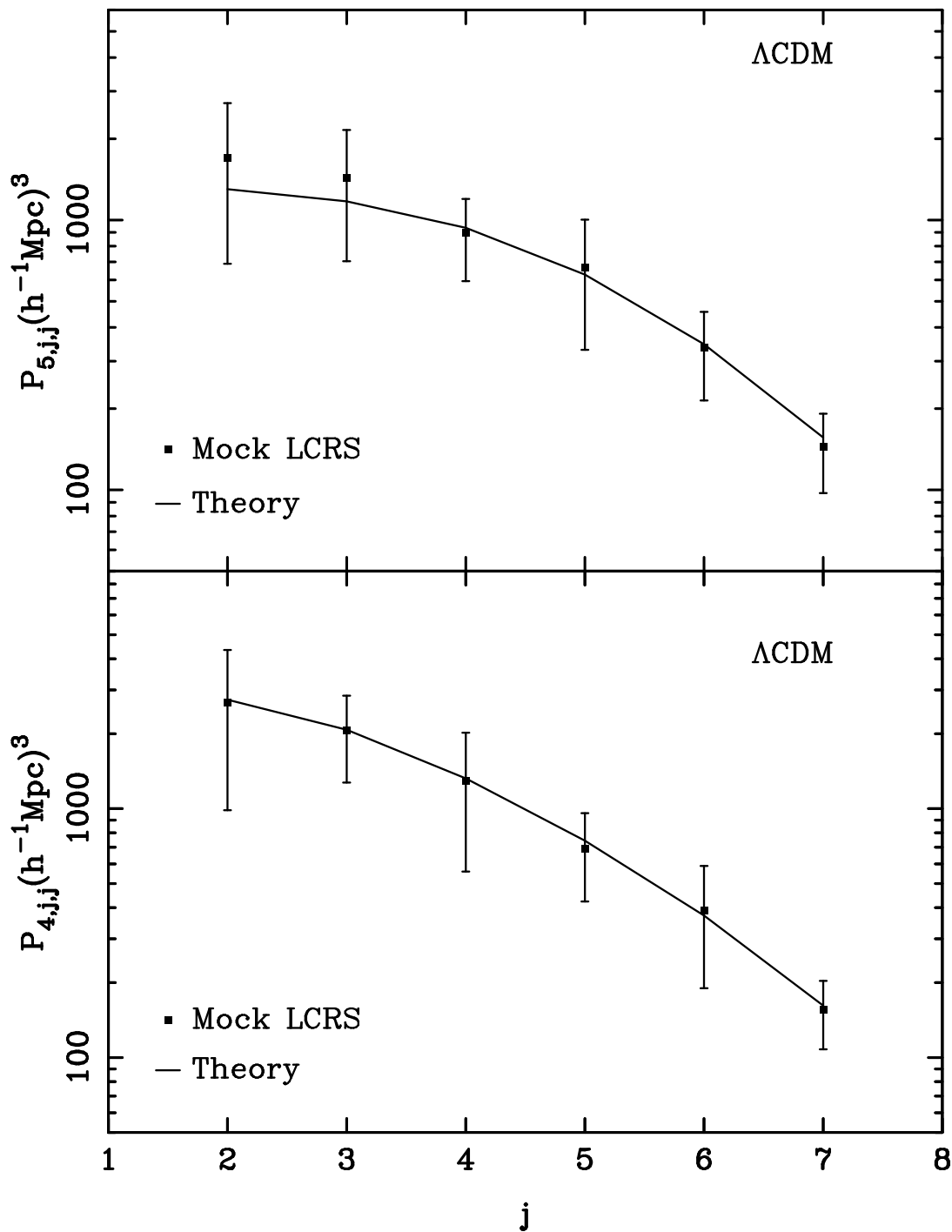


Fig. 5.— The off-diagonal DWT spectra $P_{5,j,j}$ and $P_{4,j,j}$ for Λ CDM mock LCRS samples in real space. The solid lines are the spectrum calculated by eq.(13).

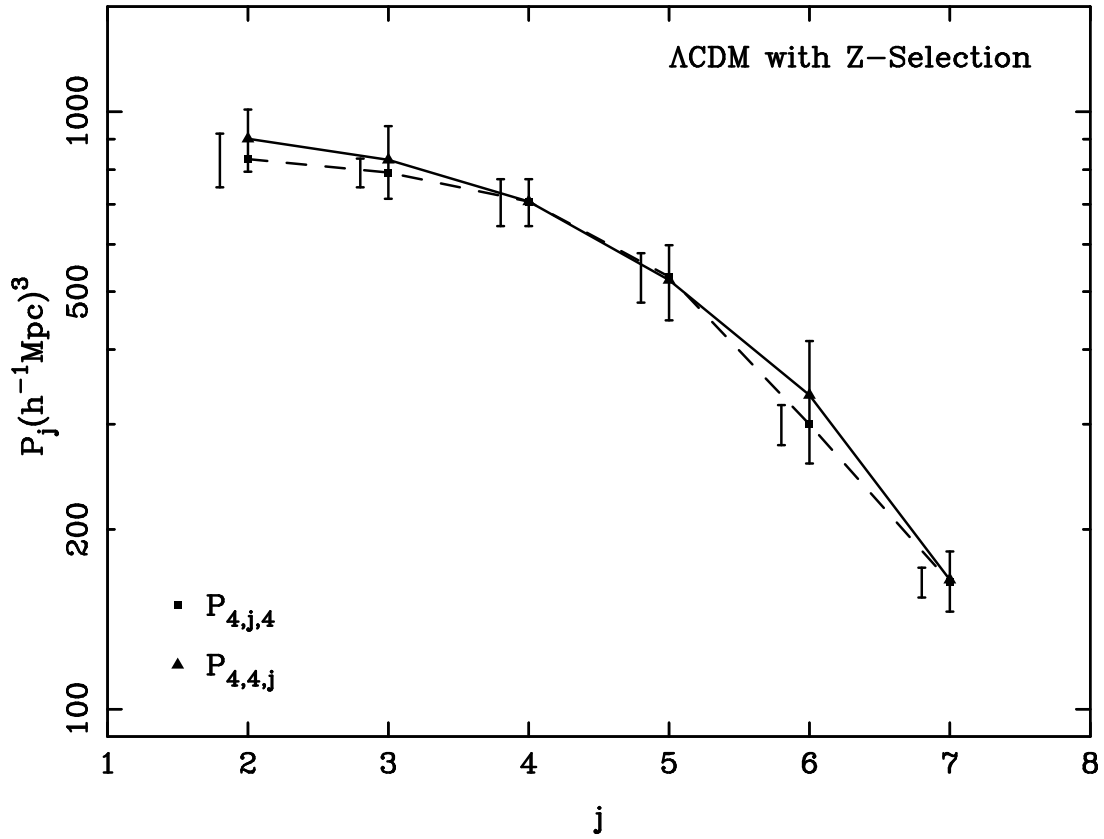


Fig. 6.— The off-diagonal power spectra P_{4j4} and P_{44j} vs. j for Λ CDM simulation sample in real space, but the selection function is taken account by plane parallel approximation. For clarity, the error bars of P_{4j4} are shifted left by a factor of 0.2.

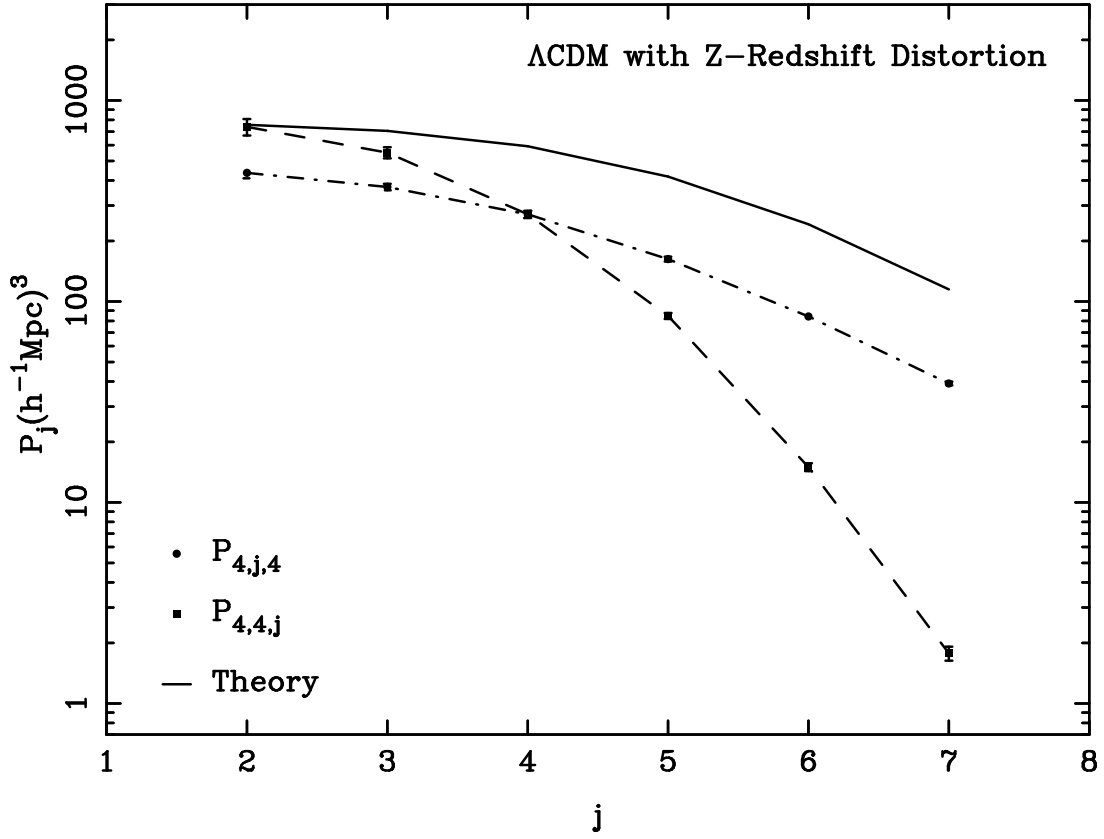


Fig. 7.— The off-diagonal power spectra P_{4j4} and P_{44j} vs. j for Λ CDM simulation sample in redshift space. The redshift distortion is taken account by plane parallel approximation. Selection function is not applied.

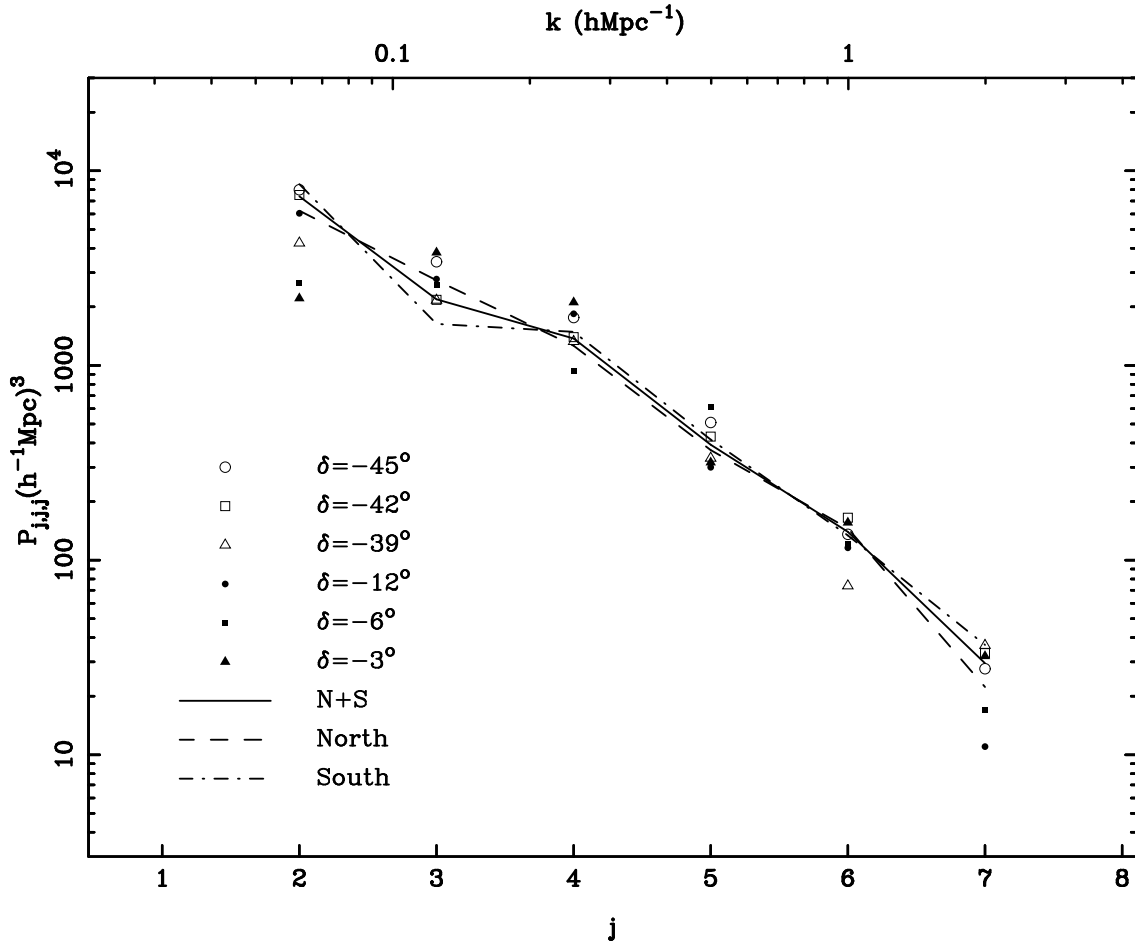


Fig. 8.— The DWT power spectrum measured in the flux-limited LCRS samples. The scatter symbols represent the DWT power spectrum measured in the six slices as indicated on the legend. The solid line show the mean power averaged over these six slices. The dash and dot-dash line are for the DWT power spectra calculated from the three north and south

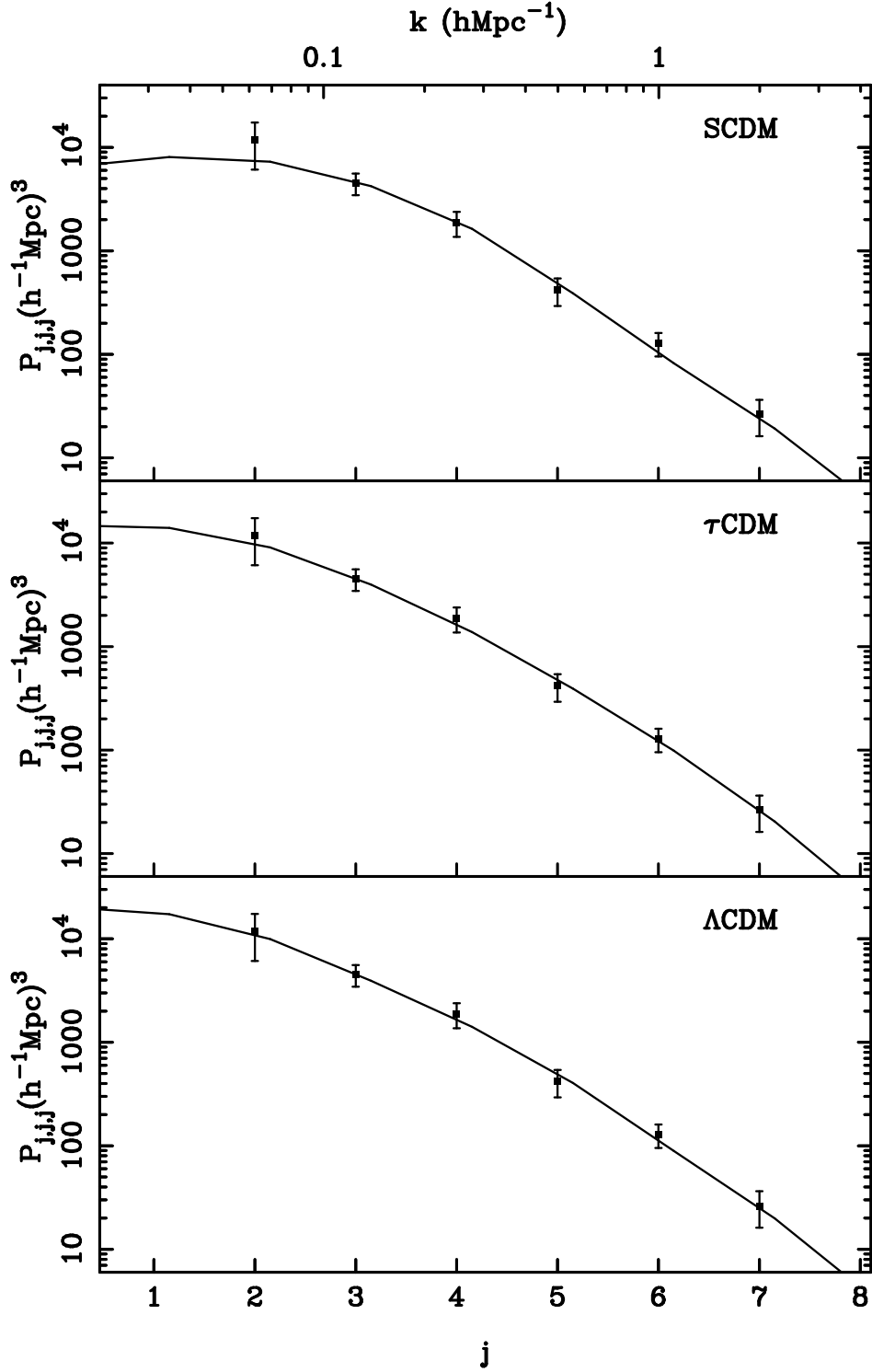


Fig. 9.— The best-fitting (solid line) of the LCRS diagonal DWT power spectrum for models SCDM (upper panel), τ CDM (central panel) and Λ CDM (lower panel) with parameters listed in Table. 1. The observed values (solid square) has been corrected for slice-like geometry effect using the mock samples. The error bars are given by $1\text{-}\sigma$ variance obtained from the

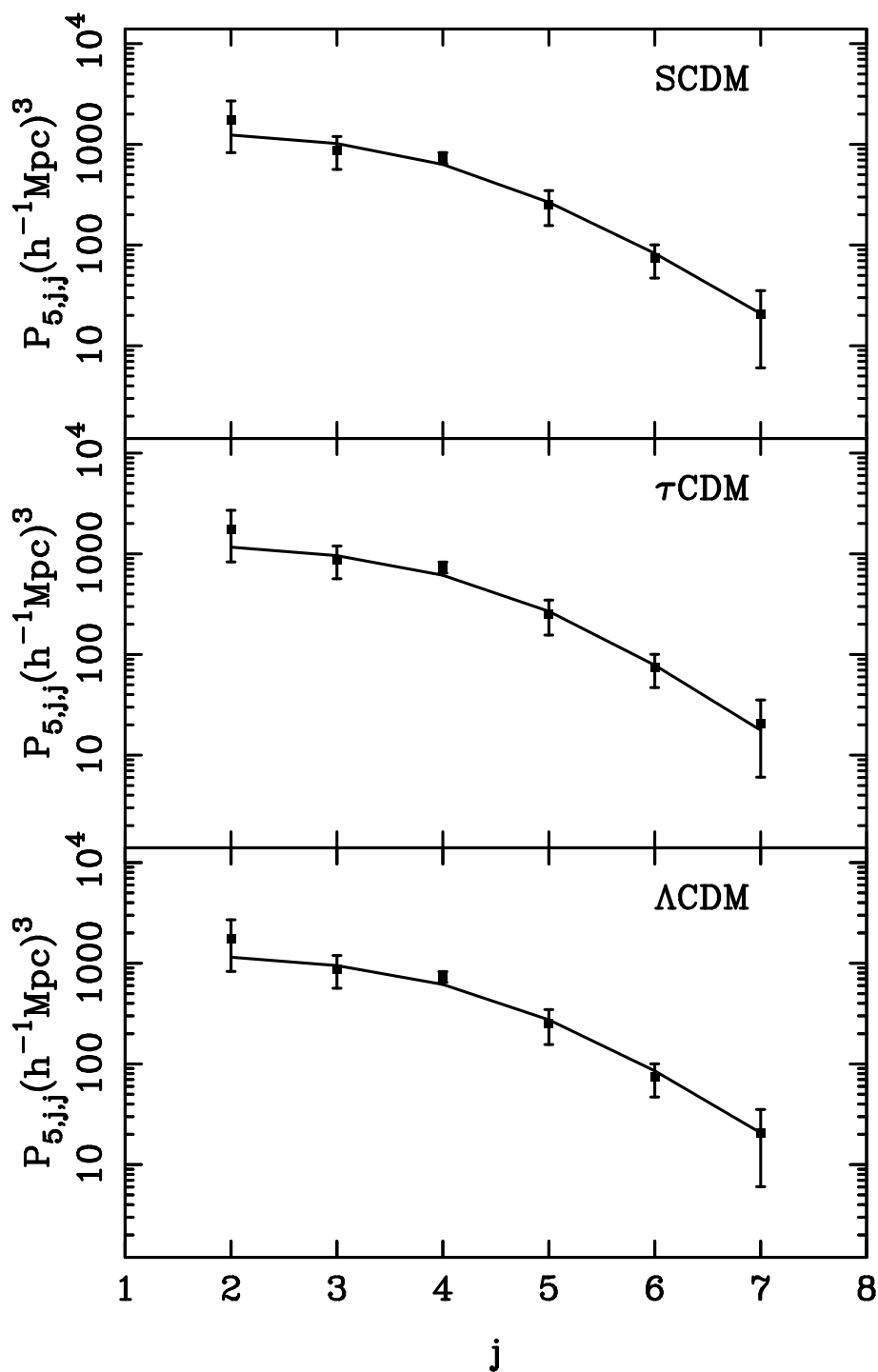


Fig. 10.— The best-fitting (solid line) of the LCRS off-diagonal power spectrum P_{5jj} for models SCDM (upper panel), τ CDM (central panel) and Λ CDM (lower panel) with parameters listed in Table. 1.